Supplementary Information

Abiotic Formation of Hexoses and Disaccharides in Aqueous Microdroplets

Myles Quinn Edwards[a], Dylan T. Holden[a], and R.Graham Cooks[a]

[a] Department of Chemistry, Purdue University, 560 Oval Drive, West Lafayette, 47907 (USA)

Table of Contents

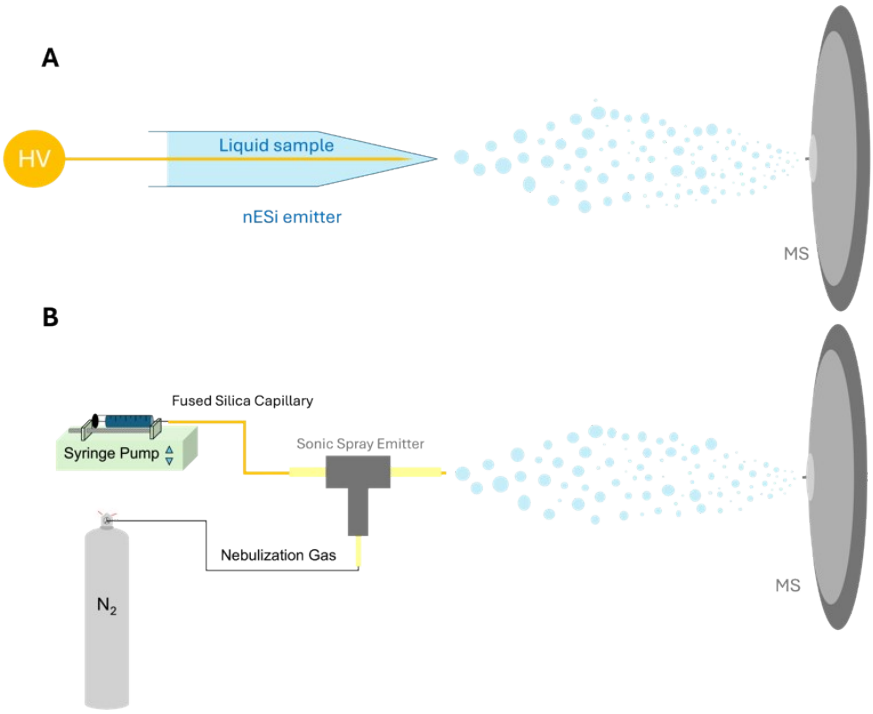

Figure S1. Ionization methods used for the present work. (A) A nESI emitter set up where a Pt wire is placed into pulled silica capillary containing the reaction solution and positioned near the MS inlet. B.) Sonic spray emitter where a nebulizing gas flow of N_2 is used to spray a fine mist from a fused silica capillary.

Supporting Information Note 1

Mass spectrometer instrument conditions:

LTQ-XL Orbitrap ESI conditions:

For electrospray ionization (ESI) on the LTQ XL Orbitrap, the source voltage was set to ±4.5 kV, with a sheath gas flow rate of 8 arb. units and both the auxiliary and sweep gas flow rates maintained at 0 arb. units. The capillary voltage was held at ±45 V, the capillary temperature was set to 275°C, and the tube lens voltage was adjusted to ±175 V.

LTQ-XL Orbitrap nESI conditions:

For nano electrospray ionization (nESI) on the LTQ XL Orbitrap, the source voltage was set to ±2 kV. The capillary voltage was held at ±45 V, the capillary temperature was set to 275°C, and the tube lens voltage was adjusted to ±175 V.

LTQ nESI Mass spectrometer settings:

A source voltage of ±2 kV was applied, with a capillary voltage of ±15 V, a capillary temperature of 275°C, and a tube lens voltage of ±65 V.

Supporting Information Note 2

Distinguishing covalent products from gas-phase adducts using in source fragmentation:

A gentle method to distinguish between noncovalent (*i.e.* proton-bound, sodium-bound) dimers and covalent products is described in the Experimental Section. When more energetic collisions were needed, as in the case of the sodium-adducted pentose disaccharide product, the operating parameters of the mass spectrometer were adjusted by increasing the voltage on the skimmer and the first multipole, imparting additional energy to ions as they are transferred through the mass spectrometer into the ion trap. At low energies, this process preferentially dissociates the weakly bound non-covalent dimers relative to the sodium bound covalent ions. By applying 30 V of in-source fragmentation energy, the only analyte peaks remaining for the pentose experiment were *m/z* 173, *m/z* 305 and a small peak at *m/z* 323. As expected, the sodium-adducted noncovalent dimer at *m/z* 323 intensity was greatly reduced, from 50% relative intensity to 1% relative intensity, with no change in the relative intensity of the sodium-bound pentose disaccharide peak *m/z* 305 (Figure S12). These results suggest the peak at *m/z* 305 represents a covalent product and not an adduct nor a dehydration product from the now-depleted sodium-bound dimer.

Furthermore, proton-bound dimers of hexose monosaccharides have been reported to produce disaccharides upon applying significant activation energy in the gas phase[1] yet little has been documented about the gas-phase production of disaccharides from sodium-bound dimers of monosaccharides. To distinguish a microdroplet reaction from a gas phase reaction, in-source fragmentation was utilized. Similar to the behaviour observed with the pentose disaccharide above, applying in-source energy significantly reduced the relative intensity of the sodium-bound dimer at *m/z* 383 from 100% to 10% at 30 V of in-source fragmentation, with a slight decrease in the *m/z* 365 peak relative intensity and large increase in the sodium bound monosaccharide from 77% to 100% relative intensity (Figure S14). Other adducts, like the ammonium adduct $[C_6H_{12}O_6+NH_4]^+$ at *m/z* 198 were completely depleted. The main peaks remaining after the applied in-source fragmentation were those at *m/z* 203 $[C_6H_{12}O_6+Na]^+$, *m/z* 365 $[C_{12}H_{22}O_{11}+Na]^+$ and a small peak of *m/z* 383 $[C_6H_{12}O_6+Na+C_6H_{12}O_6]+$. This indicates that the formation of the *m/z* 365 product likely does not occur in the gas phase from *m/z* 383 but is a microdroplet-phase reaction product.

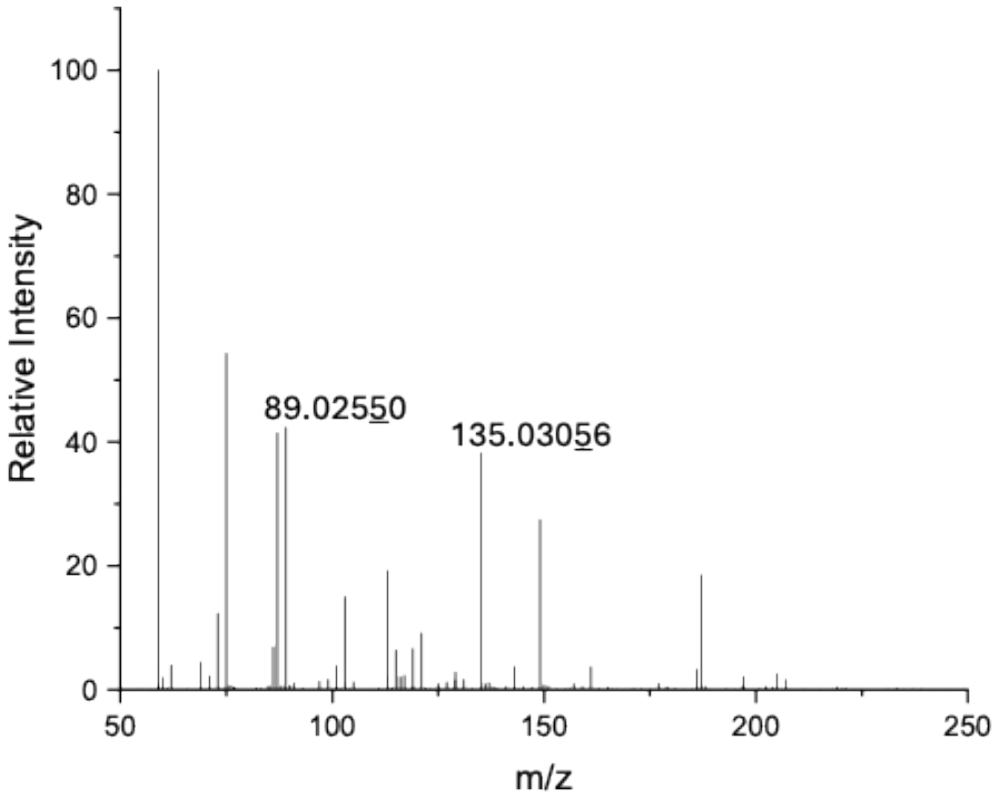

Figure S2: High resolution negative mode electrospray mass spectrum of 10 mM aqueous dihydroxyacetone where *m/z* 89 corresponds to the deprotonated analyte and *m/z* 135 corresponds to the analyte bound to a formate anion. No hexose product signal is seen at *m/z* 179.

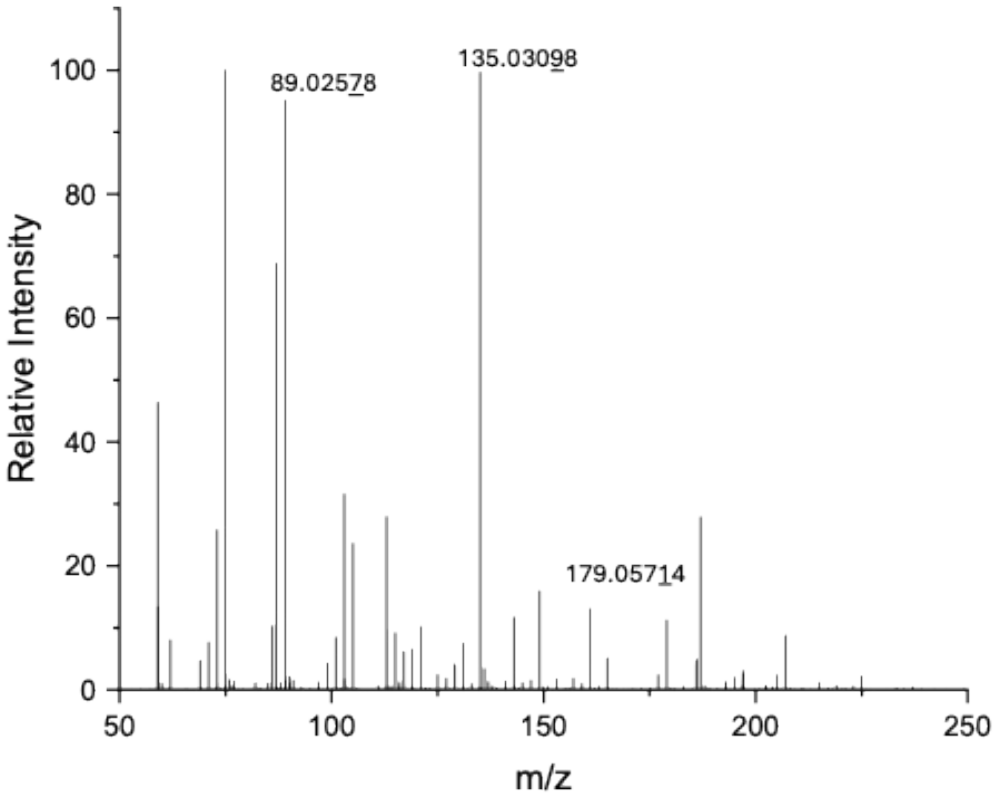

Figure S3: High resolution negative mode electrospray mass spectrum of 10 mM aqueous glyceraldehyde where *m/z* 89 corresponds to the deprotonated analyte and *m/z* 135 corresponds to the analyte bound to a formate anion. A potential hexose product peak at *m/z* 179 was noted and subjected to MS/MS to determine structure.

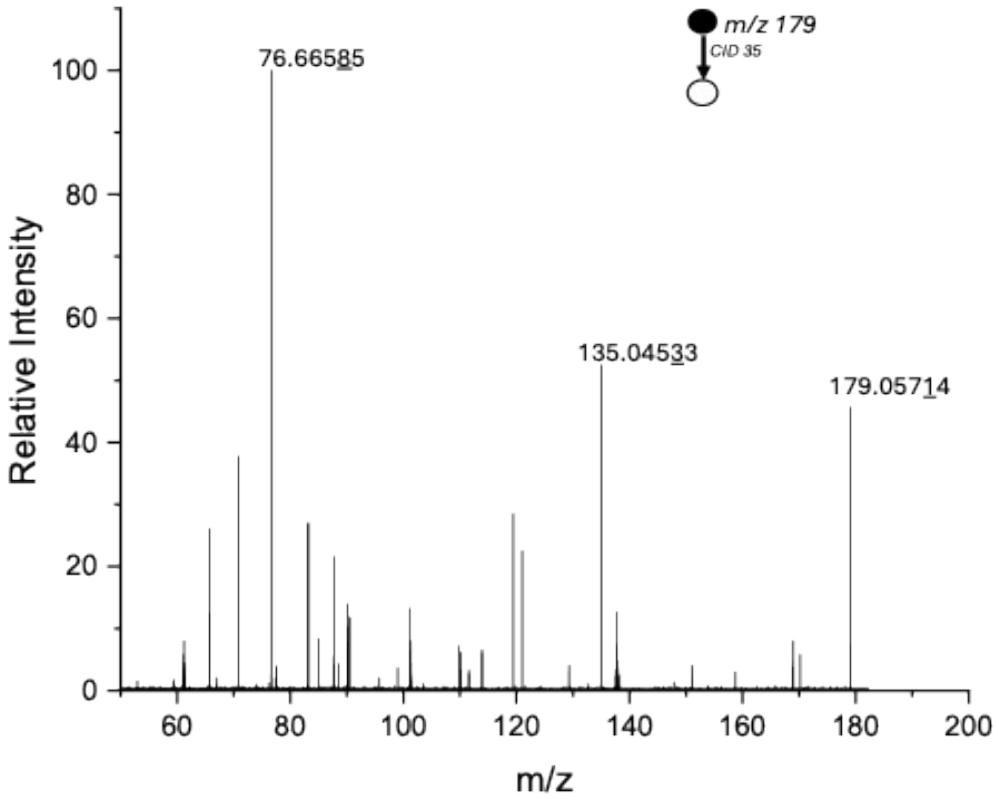

Figure S4: High resolution negative mode MS/MS of *m/z* 179 generated by electrospray ionization of 10 mM aqueous glyceraldehyde using collision energy 35 (manufacturer's unit). The most intense fragments *m/z* 135 and *m/z* 76 as well as other fragments are not known to be produced from hexoses[2].

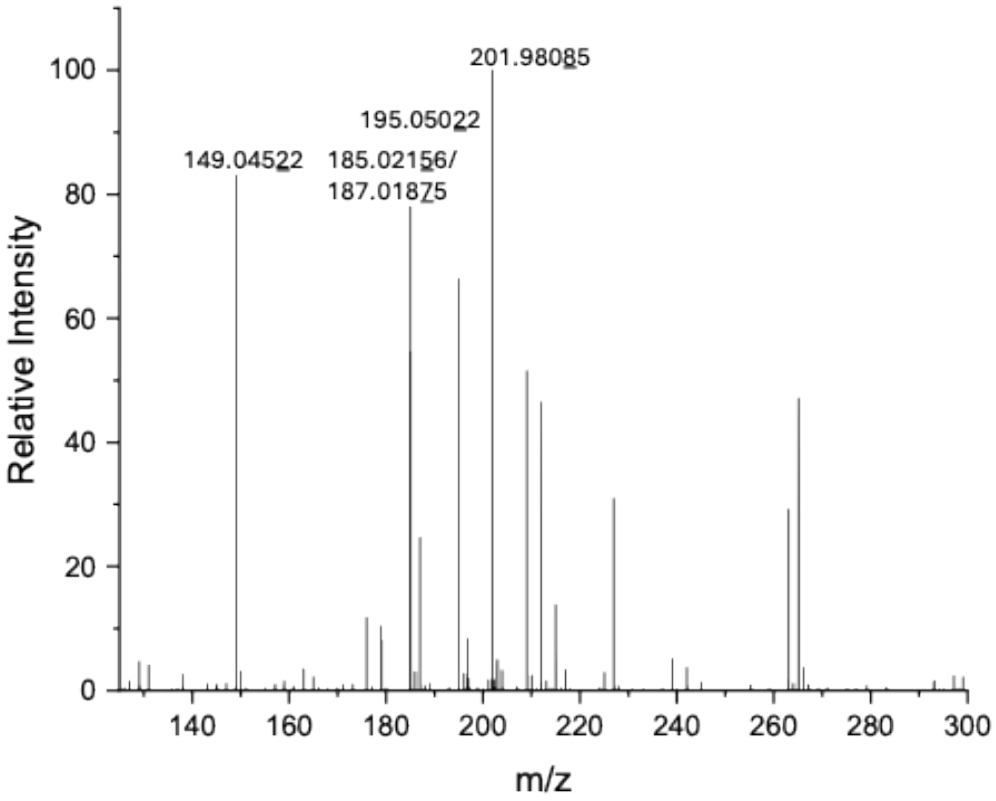

Figure S5: High resolution xylose ESI full scan mass spectrum in negative mode. The spectrum shows the deprotonated analyte at *m/z* 149, the chlorinated adduct at *m/z* 185/187, the formate adduct at 195. The peak at *m/z* 202 is a contaminant ion due to carry over. No deprotonated disaccharide product peak at *m/z* 241 was noted.

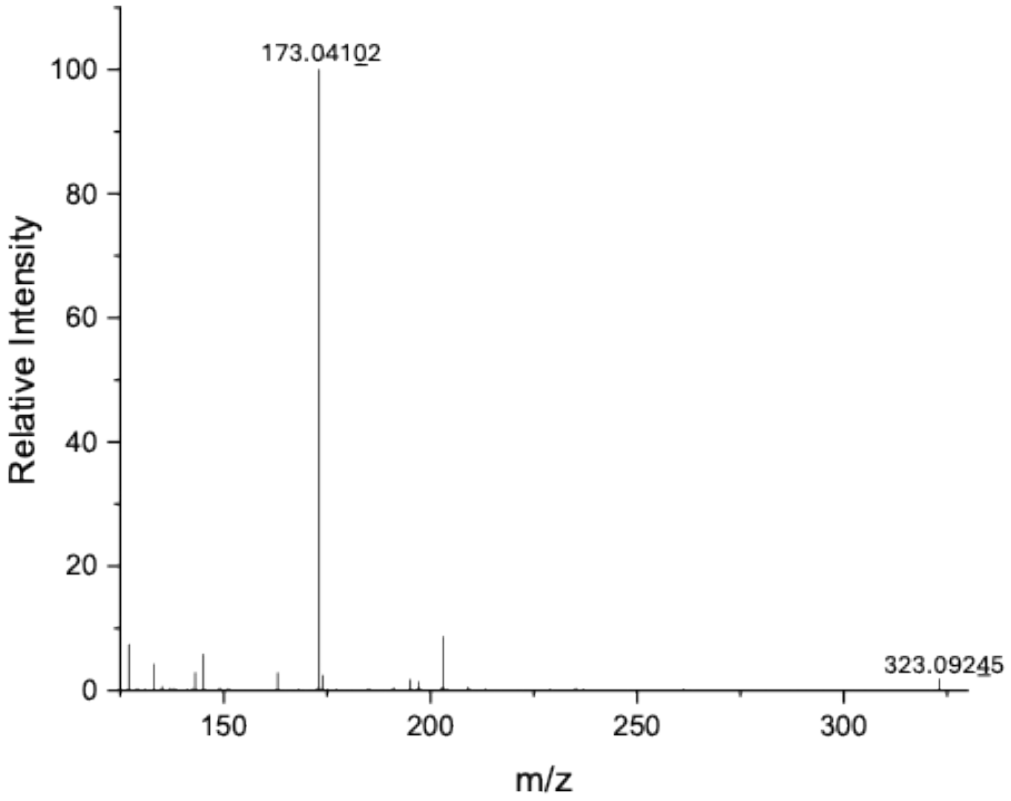

Figure S6: High resolution xylose ESI mass spectrum in positive mode. The peak at *m/z* 173 represents the sodium bound analyte with *m/z* 323 being the sodium bound dimer. No sodium bound disaccharide product peak at *m/z* 305 was noted.

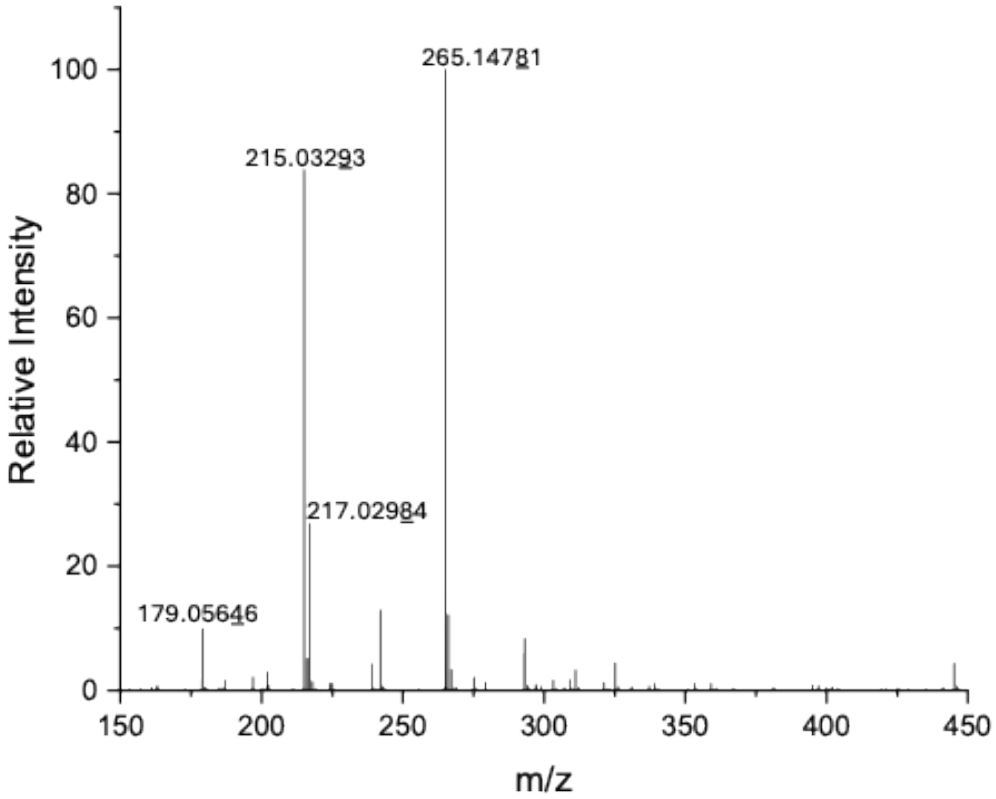

Figure S7: High resolution glucose ESI mass spectrum in negative mode. The spectrum shows the deprotonated analyte at *m/z* 179, the chlorinated adduct at *m/z* 215/217. The peak at *m/z* 265 is a contaminant ion eluted from the spray tubing. No deprotonated hexose disaccharide product peak at *m/z* 341 was noted.

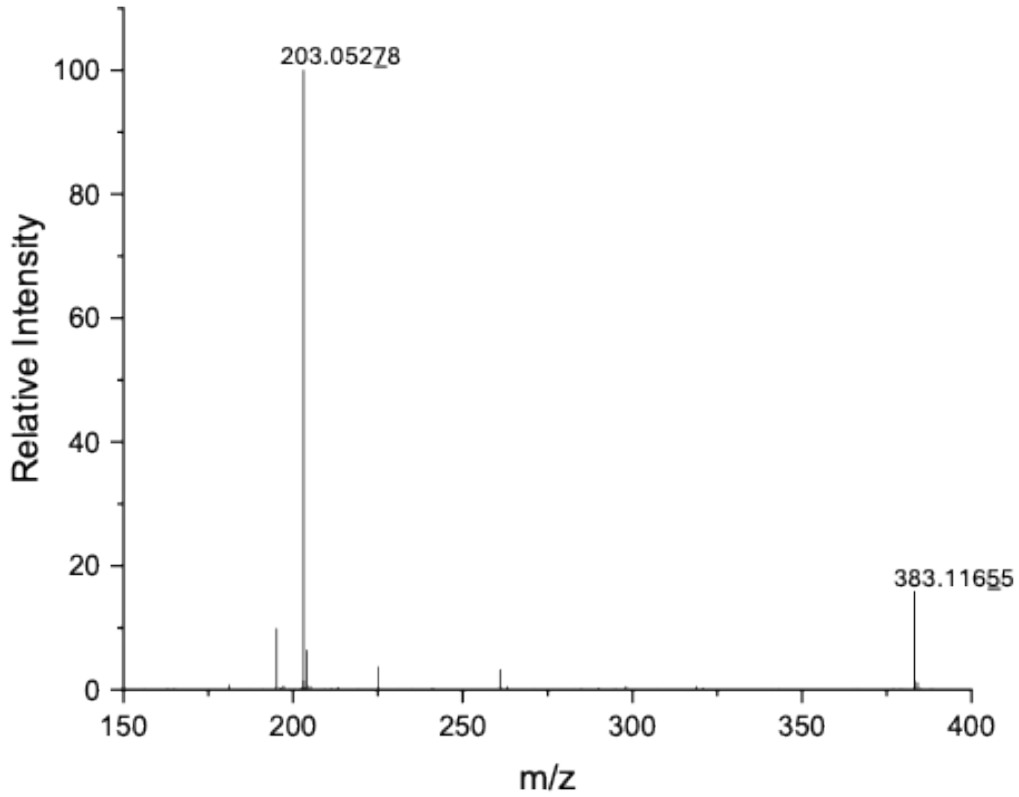

Figure S8: High resolution glucose ESI mass spectrum in positive mode. The peak at *m/z* 203 represents the sodium bound analyte with *m/z* 383 being the sodium bound dimer. No sodium bound hexose disaccharide product peak at *m/z* 365 was noted.

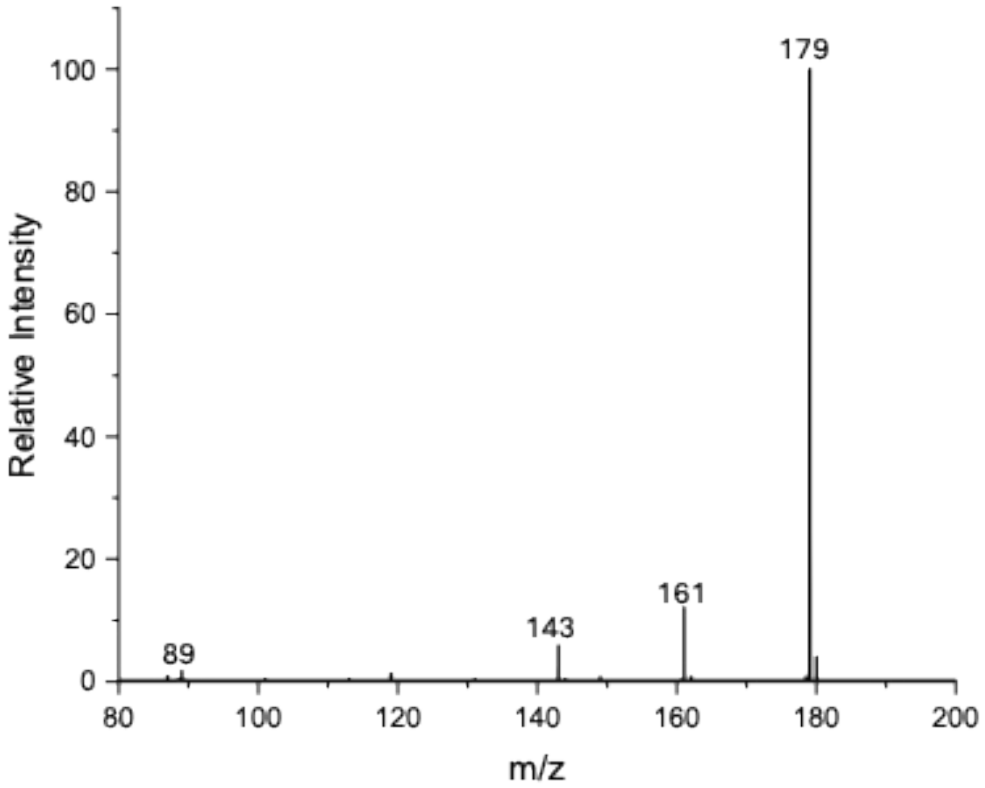

Figure S9: High resolution negative mode nanoelectrospray mass spectrum of 10mM aqueous dihydroxyacetone recorded using a Q-ToF with nominal mass *m/z* 179 being the ion of interest and nominal mass *m/z* 89 being the deprotonated analyte.

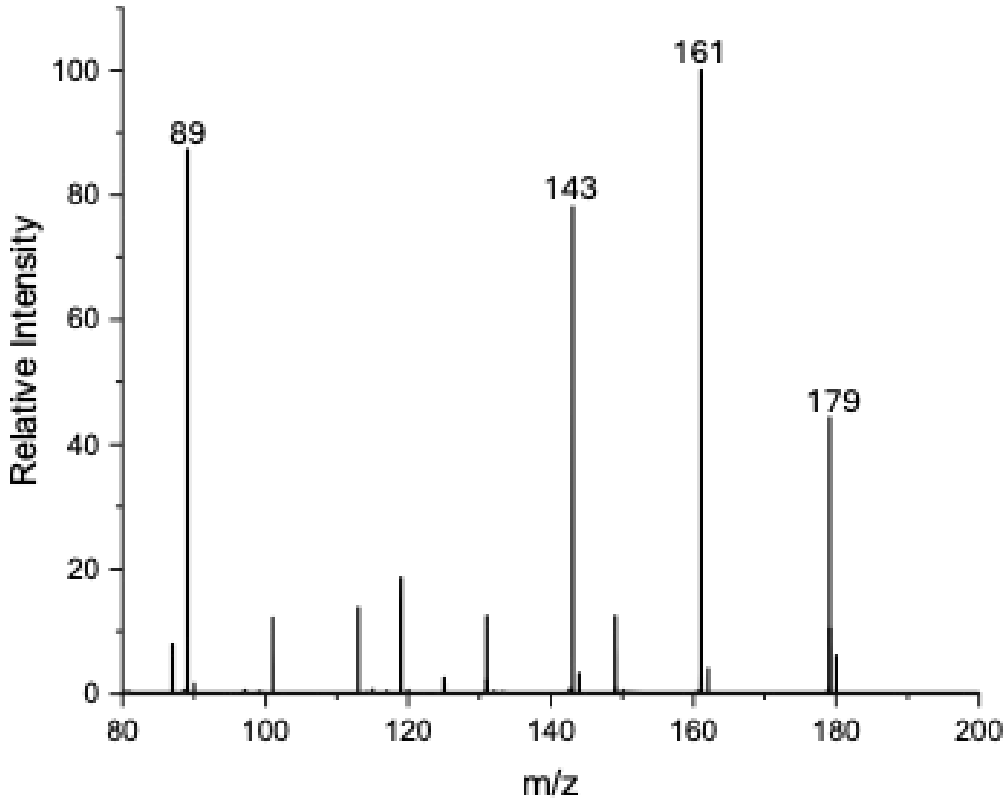

Figure S10: High resolution negative mode nanoelectrospray mass spectrum of 10 mM aqueous glyceraldehyde recorded using a Q-ToF with nominal mass *m/z* 179 being the ion of interest and nominal mass *m/z* 89 being the deprotonated analyte.

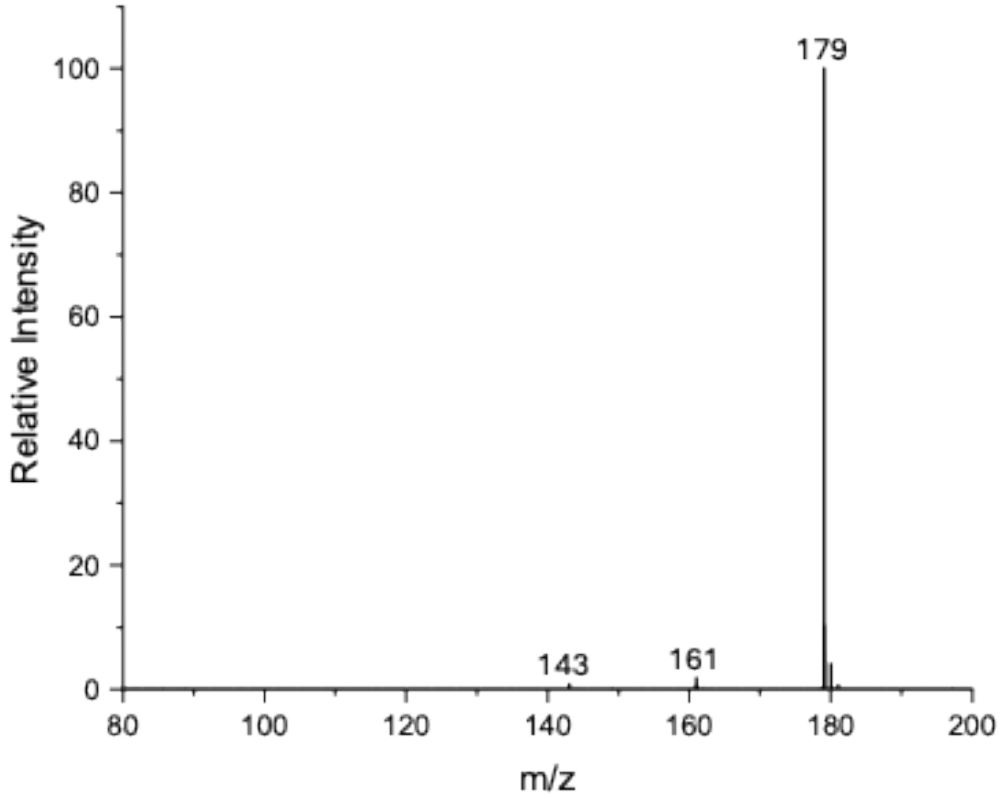

Figure S11: High resolution negative mode nanoelectrospray mass spectrum of 10 mM aqueous sorbose recorded using a Q-ToF with nominal mass *m/z* 179 being the analyte of interest.

Table S1: Experimental Exact masses of Hexose Formation

Identity	Experimental Exact Mass*	Locked Mass	Error (ppm)
Sorbose/Fructose	179.05604	179.0560401	N/A
Dihydroxyacetone Product	179.05546	179.0560401	-3.18
Glyceraldehyde Product	179.05568	179.0560401	-1.95

*The underline represents the last significant digit

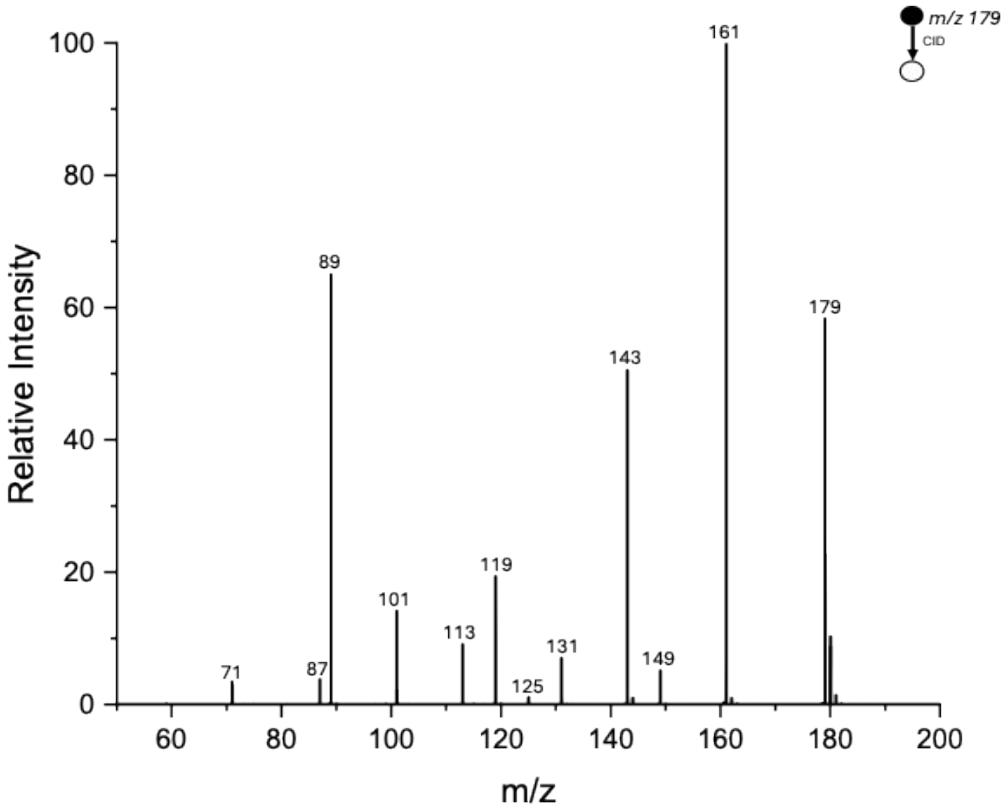

Figure S12: High resolution negative mode nanoelectrospray MS/MS spectrum of 10 mM aqueous fructose recorded using a Q-ToF.

Supporting Information Note 3

Hexose Fragmentation:

The species at *m/z* 179 undergoes a neutral loss of 18 Da (H_2O), yielding the fragment at *m/z* 161, a common dehydration process in carbohydrates. Further neutral losses include 30 Da (formaldehyde, CH_2O) forming *m/z* 149, and 48 Da (CH_4O_2) producing *m/z* 131. Neutral loss of 60 Da ($C_2H_4O_2$) results in *m/z* 119, while a 64 Da loss (CH_4O_3) forms *m/z* 115. Neutral loss of 66 Da (CH_4O_2) produces m/z 113, and 78 Da ($C_2H_6O_3$) yields *m/z* 101. Lastly, a 90 Da loss ($C_3H_6O_3$) generates *m/z* 89, indicative of a triose fragment. This fragmentation pattern matches previously reported literature data for other negative mode sugar fragments.[2]

Supporting Information Note 4:

Positively charged and negatively charged droplets:

Without an externally applied potential, microdroplets can exhibit a net positive or negative charge.[34] In fact, even in electrospray experiments the charge in a small fraction of droplets is opposite in sign of the applied potential.[5] Thus, microdroplets can simultaneously have properties of both a net negative and net positive charge. One example of this phenomenon is the pH gradient[6,7] within microdroplets and the basic or acidic layers[3] providing activating conditions and a pathway to catalyst-free reactions. This means that it is possible to have reactions occurring in the double layer leading to an acid catalysis in negative mode.

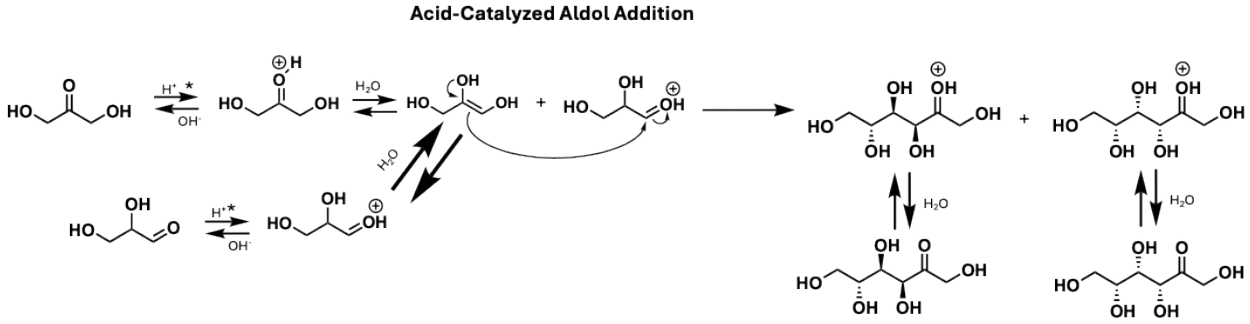

Scheme S1: Acid-catalyzed aldol addition of glyceraldehyde and dihydroxyacetone to form fructose and sorbose.

\

Table S2: Experimental Exact masses of Disaccharide Formation

Identity	Experimental Exact Mass*	Theoretical Mass	Error (ppm)
Glucose product (+)	365.10449	365.105433	-2.58
Glucose product (-)	341.10781	341.108935	-3.30
Xylose product (+)	305.08355	305.084303	-2.47
Xylose product (-)	281.08643	281.087806	-4.90

*The underlining represents the last significant digit

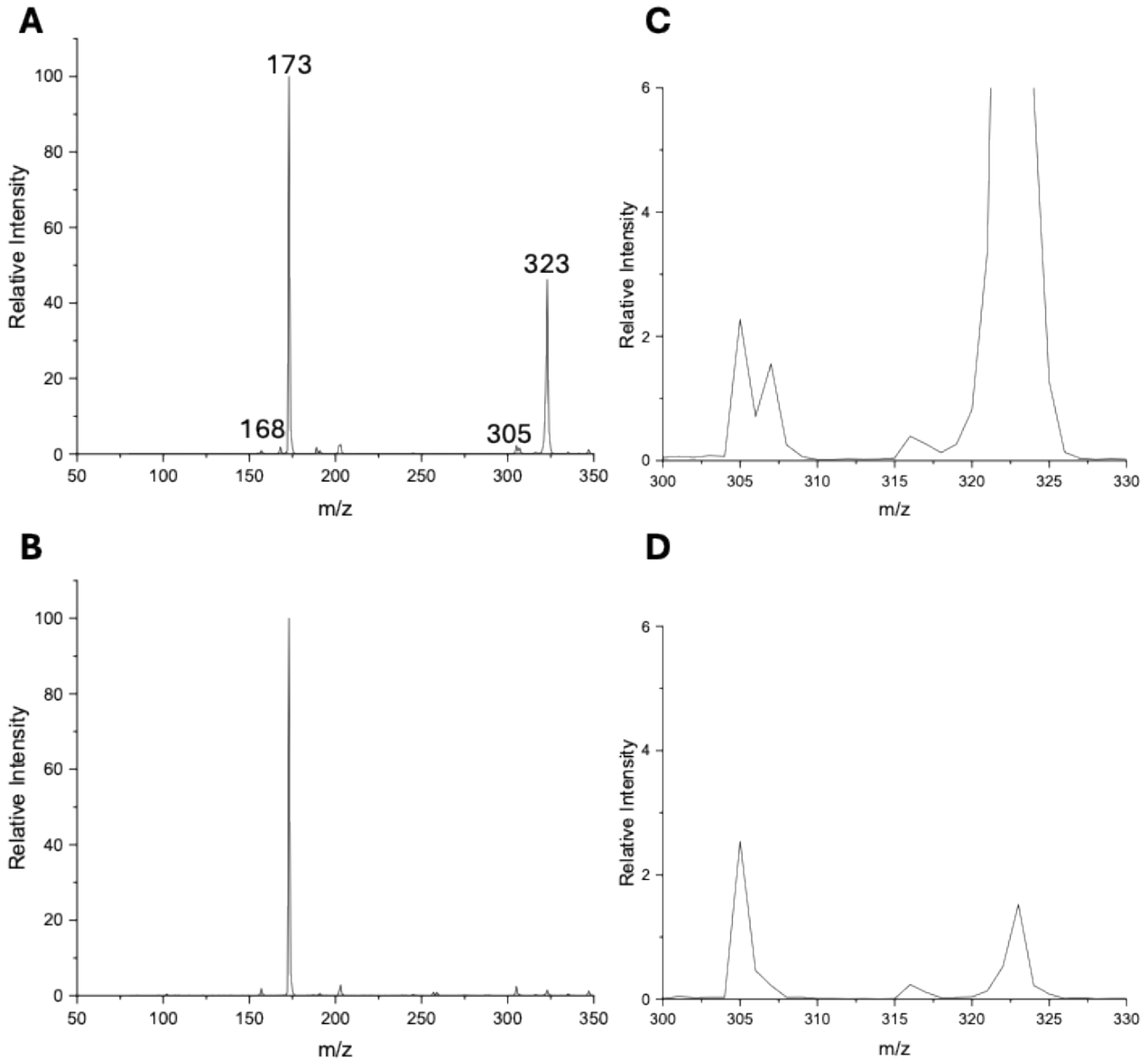

Figure S13: Full scan mass spectra of xylose. **A.** Full scan mass spectrum of xylose with no in-source fragmentation applied. **B.** Full scan mass spectrum of xylose with 30V in-source fragmentation applied. **C.** Zoom-in onto peaks of interest with no in-source fragmentation. **D.** Zoom in of peak peaks of interest with 30V in-source fragmentation applied.

Supporting Information Note 5

Pentose Disaccharide Fragmentation:

MS/MS was used to probe the structure of the potential pentose disaccharide products at *m/z* 305 shown in Figure 2. The fragmentation begins with the loss of 18 Da (H_2O), resulting in the *m/z* 287 ion. This is accompanied by the loss of 30 Da (CH_2O) to produce *m/z* 275. The most abundant product ion population at *m/z* 245 results from a neutral loss of 60 Da ($C_2H_4O_2$), while a 90 Da loss ($C_3H_6O_3$) produces m/z 215. Further fragmentation results in a 120 Da loss ($C_4H_8O_4$) to make *m/z* 185. Glycosidic cleavages are evident from the formation of two product peaks, *m/z* 173, resulting from a 132 Da loss ($C_5H_8O_4$), and *m/z* 155 likely corresponds to a consecutive 18 Da neutral loss of water from the *m/z* 173 ions. These fragments arise from the cleaving both the reducing or nonreducing side of the glycosidic bond. Cross ring cleavages combined with the glycosidic bond cleavages match previously reported fragmentation for pentose disaccharides.[8]

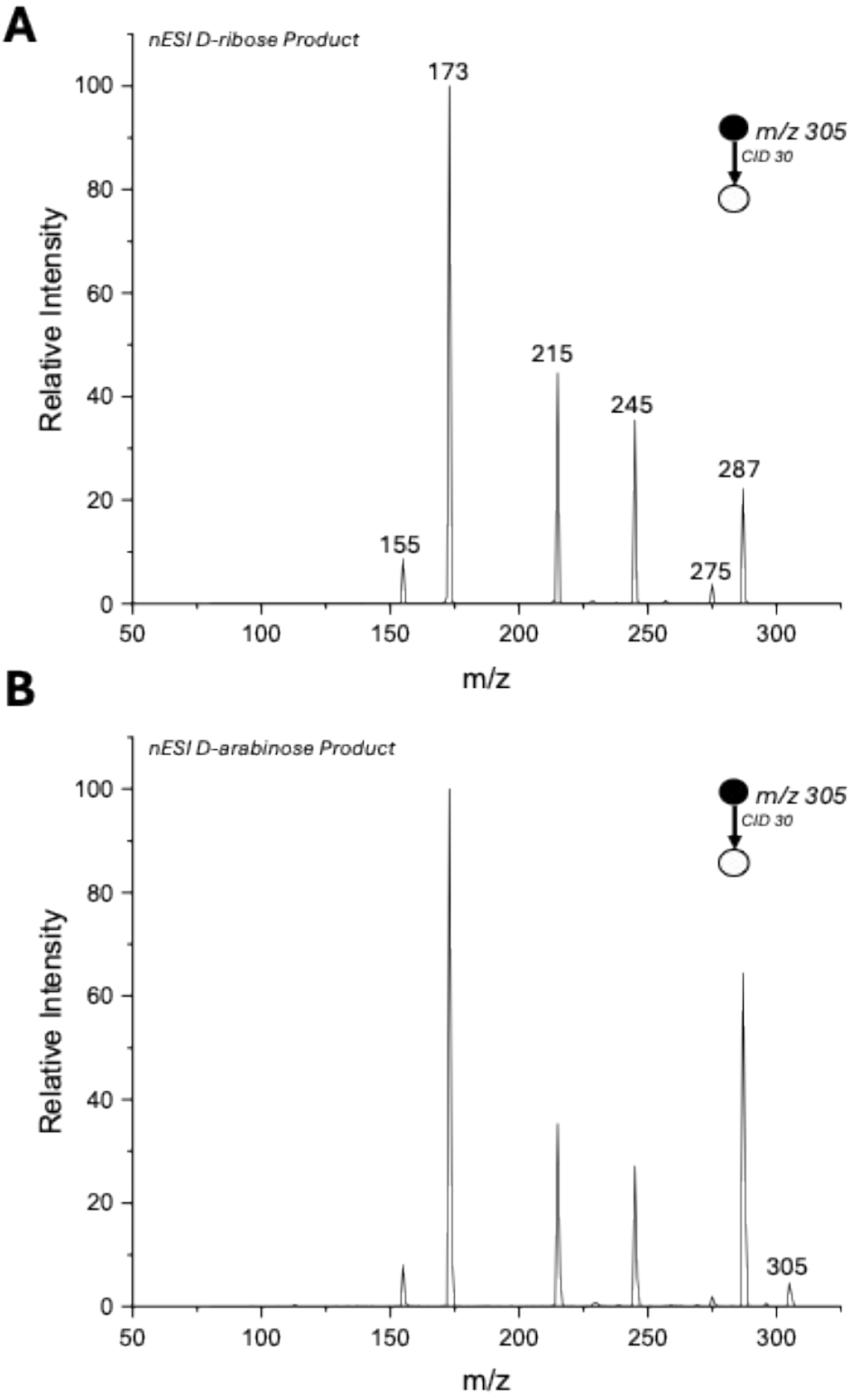

Figure S14: MS/MS of the pentose disaccharide ions *m/z* 305 generated by nESI from (**A**) ribose and (**B**) arabinose. Spectra were collected at CID 30 (manufacturer's unit).

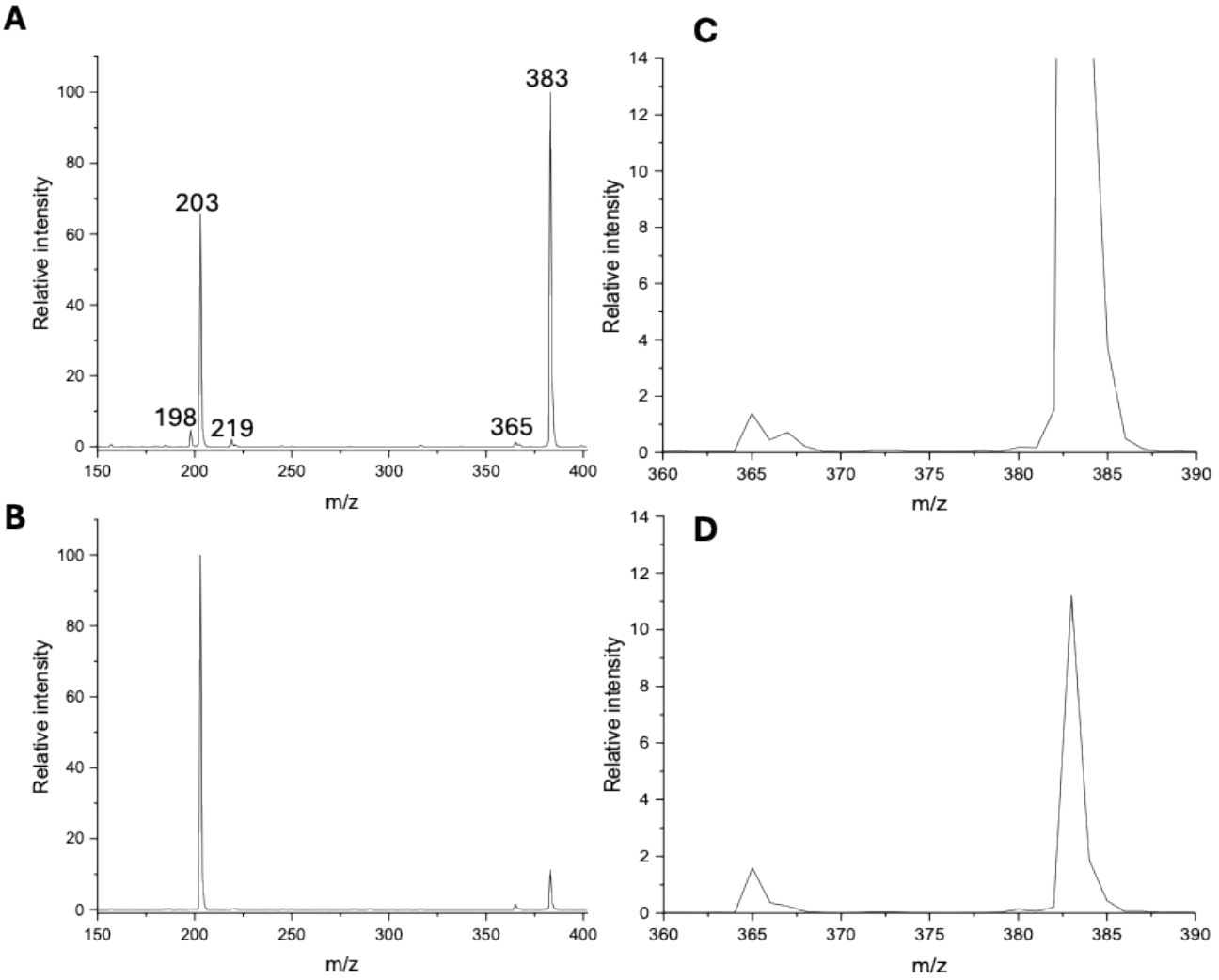

Figure S15: Full scan mass spectra of glucose. **A.** Full scan mass spectrum of glucose with no in-source fragmentation applied. **B. F**ull scan mass spectrum with 30V in-source fragmentation applied. **C.** Zoom in of peak peaks of interest with no in-source fragmentation. **D.** Zoom in of peak peaks of interest with 30V in-source fragmentation applied.

Supporting Information Note 6

Hexose Disaccharide Fragmentation:

MS/MS was used to further characterize the *m/z* 365 ion population, as shown in Figure 3. The fragment ion at *m/z* 347 $[C_{12}H_{20}O_{10}+Na]^+$ results from the loss of one molecule of water (H_2O) from the parent disaccharide ions. The fragment at *m/z* 335 $[C_{11}H_{20}O_{10}+Na]^+$ is formed through the neutral loss of a formaldehyde molecule (CH_2O), suggesting cross-ring cleavage within a single hexose unit. The fragment at *m/z* 305 $[C_{10}H_{18}O_9+Na]^+$ results from the loss of 60 Da ($C_2H_4O_2$) speculated to be loss of an ethene diol isomer,[9,10] pointing towards further ring cleavage and rearrangements. The fragment at *m/z* 275 $[C_8H_{14}O_7+Na]^+$ arises from a 90 Da loss ($C_3H_6O_3$) speculated to be a neutral loss of a propene triol isomer.[9] The fragment at m/z 203 $[C_6H_{12}O_6+Na]^+$ is produced by the loss of an entire hexose unit ($C_6H_{10}O_5$) from the disaccharide stabilized by the sodium ion.[2,9,10] The observation of this fragment is indicative of glycosidic bond cleavage. The fragment at *m/z* 185 $[C_6H_{10}O_5+Na]^+$ is formed by dissociation of the glycosidic bond and subsequent dehydration of the hexose fragment which potentially leads to a double bond or epoxide formation within the sugar structure.[9,10] The fragment ions reported are consistent with those observed for sodium-bound hexose disaccharides[2,10,11] indicating the increased likelihood of a covalent product.

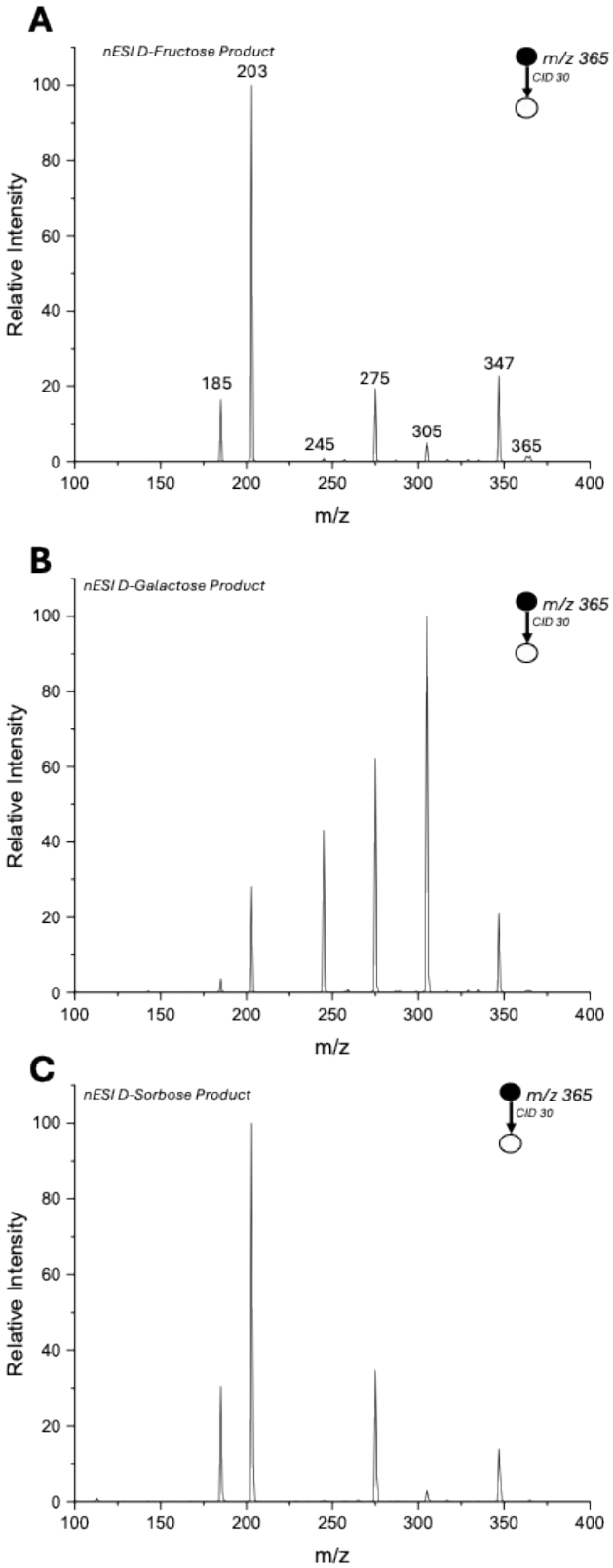

Figure S16: MS/MS of hexose disaccharide ions *m/z* 365 generated by nESI from (**A**) D-fructose and (**B**) D-galactose (**C**) D-sorbose. Spectra were collected at CID 30 (manufacturers unit).

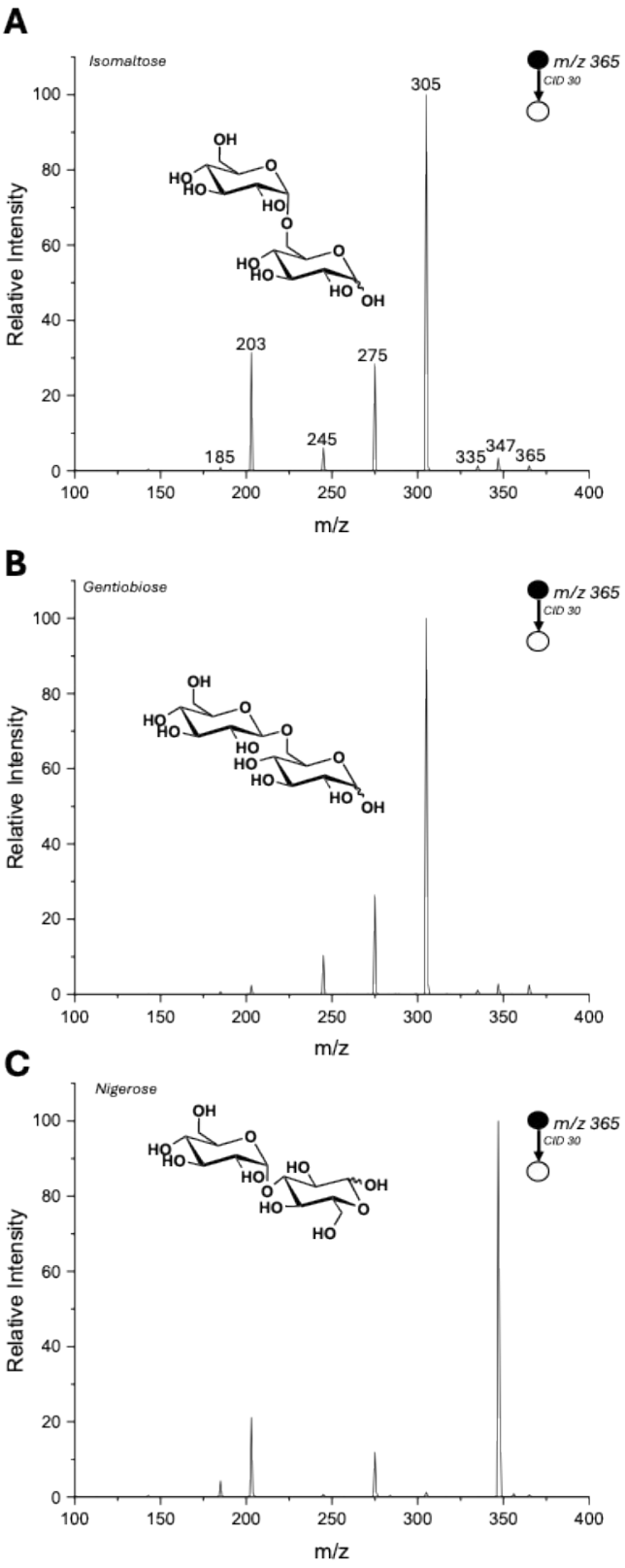

Figure S17*:* MS/MS of the ion having *m/z* 365 generated by nESI from: (**A**) isomaltose, (**B**) gentiobiose, and (**C**) nigerose. Spectra were collected at CID 30 (manufacturers unit).

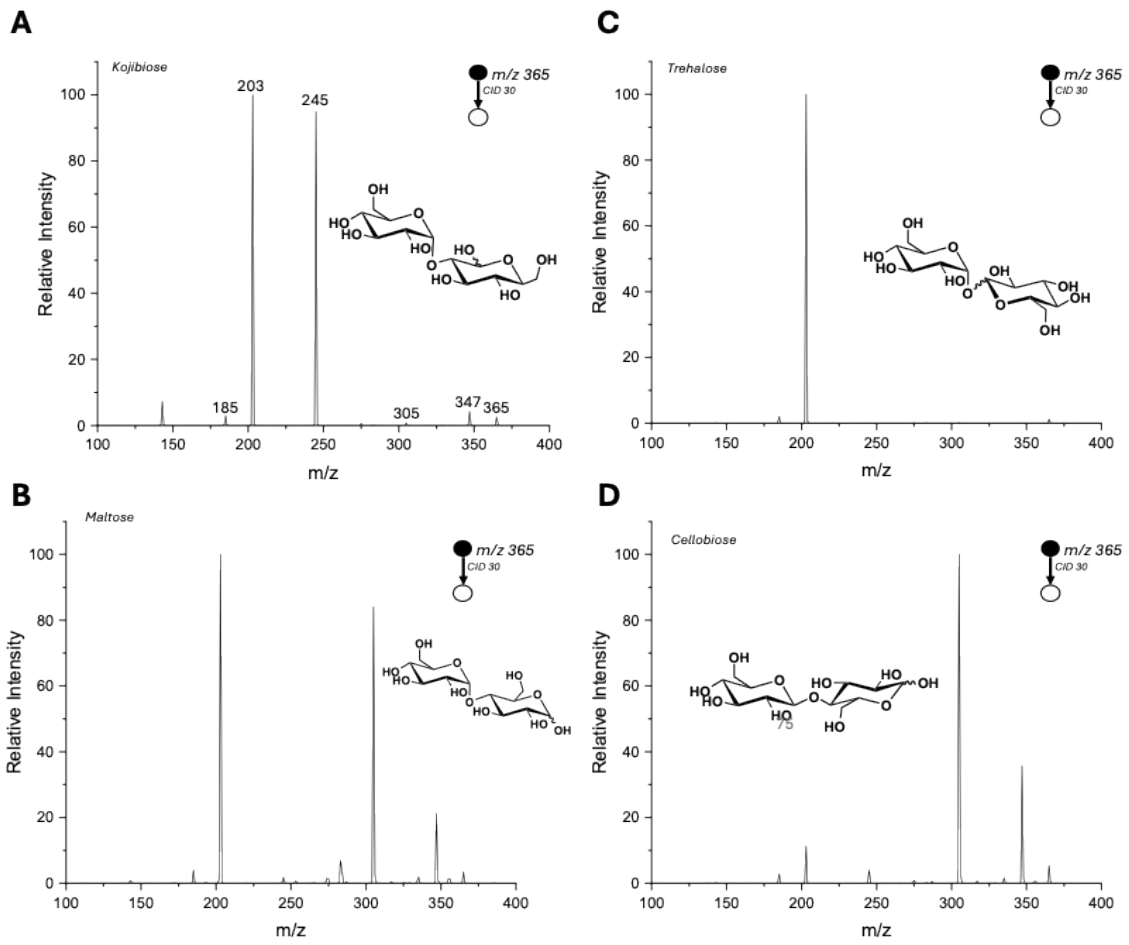

Figure S18: MS/MS of the ion having *m/z* 365 generated by nESI from (**A**) kojibiose ,(**B**) maltose, (**C**) trehalose and (**D**) cellobiose. Spectra were collected at CID 30 (manufacturers unit).

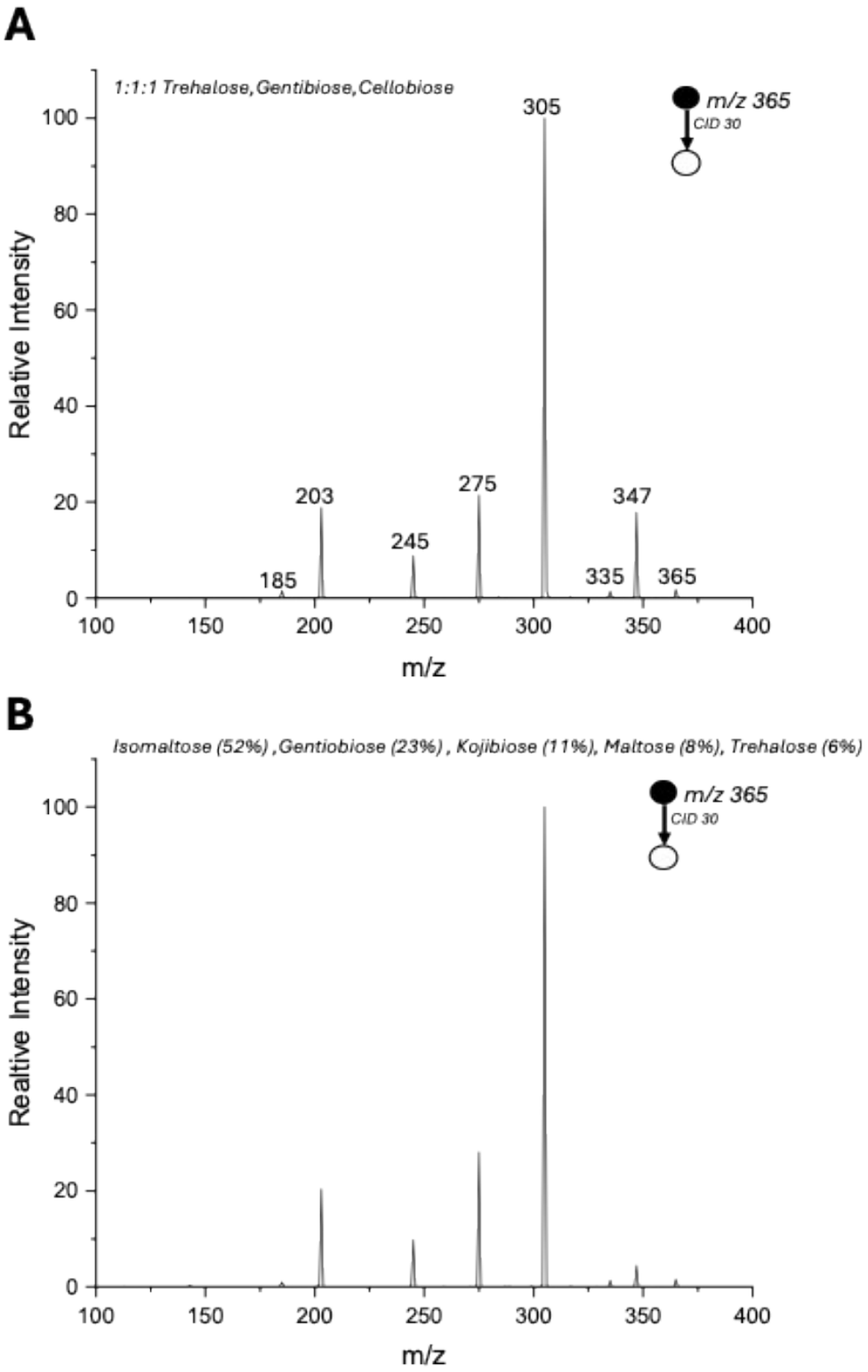

Figure S19: MS/MS of the ion having *m/z* 365 generated by nESI from (**A**) 1:1:1 mixture of trehalose, gentibiose, and cellobiose, (**B**) Mixture of isomaltose (52% v/v) ,gentiobiose (23% v/v) , kojibiose (11% v/v), maltose (8% v/v),and trehalose (6% v/v) all stock solutions were equimolar at 10mM before mixing. Spectra were collected at CID 30 (manufacturers unit).

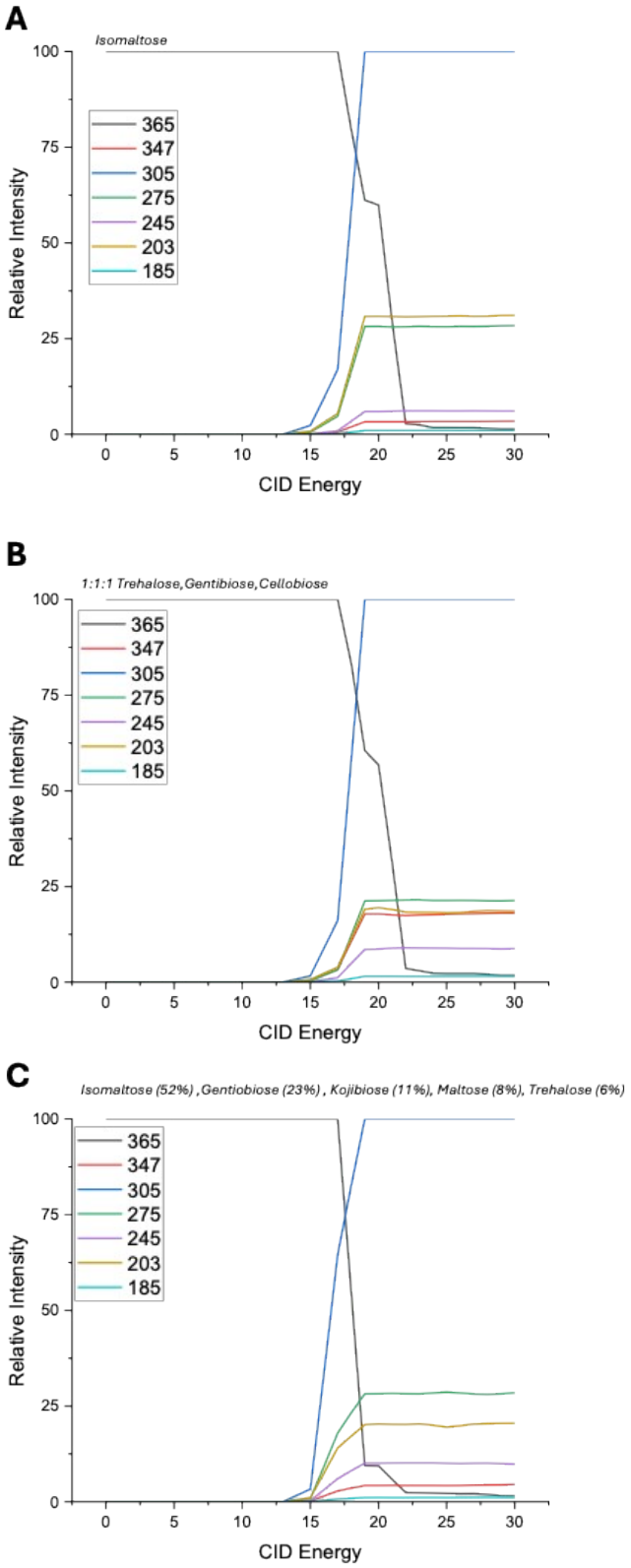

Figure S20: Breakdown curves for (**A)** Isomaltose, (**B**) 1:1:1 mixture of trehalose, gentibiose, and cellobiose, (**C**) Mixture of isomaltose (52% v/v) ,gentiobiose (23% v/v) , kojibiose (11% v/v), maltose (8% v/v),and trehalose (6% v/v). All stock solutions were equimolar at 10mM before mixing.

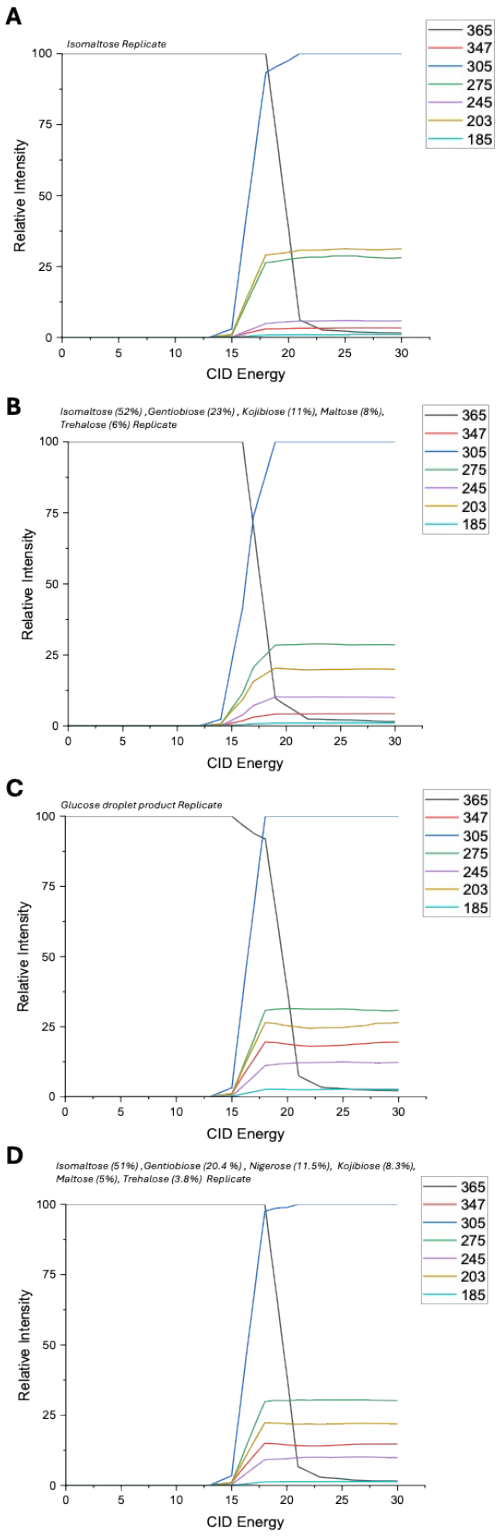

Figure S21: Breakdown curves for technical replicates of (**A**) Isomaltose, (**B**) A mixture of isomaltose (52% v/v), gentiobiose (23% v/v) , kojibiose (11% v/v), maltose (8% v/v),and trehalose (6% v/v) (**C**) The glucose droplet product (**D**) A mixture of isomaltose (51% v/v) ,gentiobiose (20.4% v/v) , nigerose (11.5% v/v), kojibiose (8.3% v/v), maltose (5% v/v),and trehalose (3.8% v/v). All stock solutions were equimolar at 10mM before mixing.

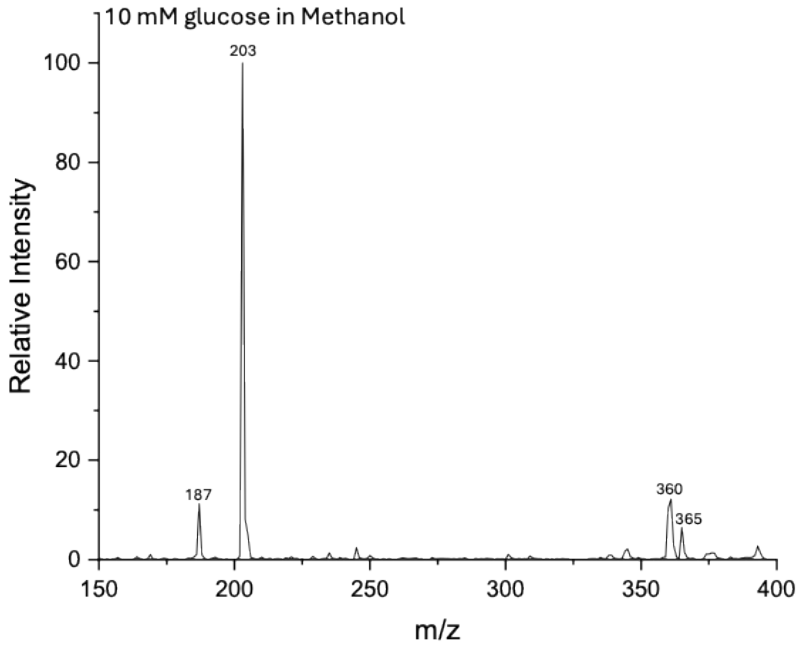

Figure S22*:* A full scan mass spectrum of 10mM glucose in methanol with 30V in-source excitation applied. Peak *m/z* 365 represents the disaccharide product while *m/z* 360 and 187 are side products. As expected, the reaction produced a greater relative intensity of disaccharide as well as side products

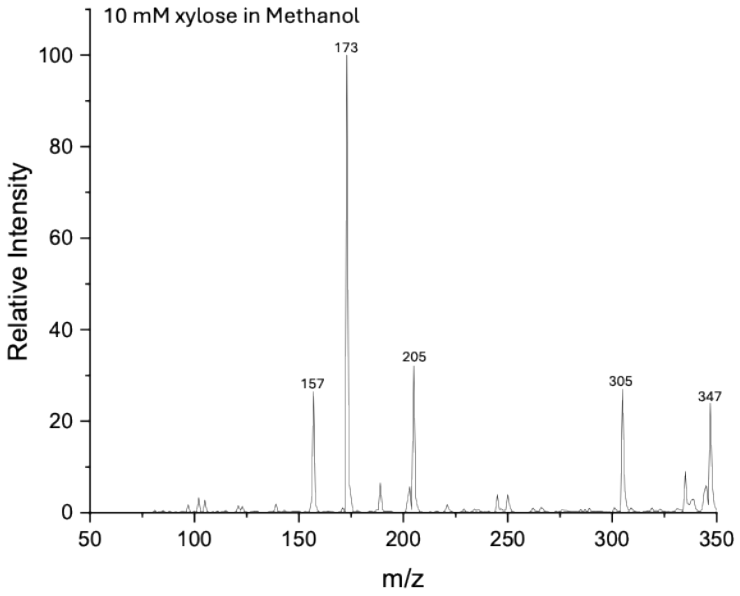

Figure S23: A full scan mass spectrum of 10mM xylose in methanol with 30V in-source excitation applied. Peak *m/z* 305 represents the disaccharide product while *m/z* 157 and 347 are side products with *m/z* 205 being a known contaminant peak of a sodium bound polymer. As expected, produced a greater relative intensity of disaccharide as well as side products.

Supporting Information Note 7

Hexose Disaccharide Quantitation:

An internal standard of 2,4,6-trimethylpyrylium tetrafluoroborate was used alongside a glucose disaccharide standard mixture with varying concentrations in 100mM salt water to create a standard curve relating the ratio of internal standard to glucose disaccharide. The plot was fit with a linear curve that had the equation y = 0.00518 ± 0.0001 1/mM (x) + 0.0317 ± 0.004 with an R^2 = 0.997. To quantitate reaction progress sonic spray was used with two different silica capillary inner diameters. The syringe was filled with 250 µL of 10 mM aqueous glucose and sprayed at a rate of 10 µL/min with 100 psi backing gas pressure for a total of 25 minutes. Reactions were sprayed into a plastic vial and 10 µL of captured spray was mixed with 10 µL of spiked internal standard mix.

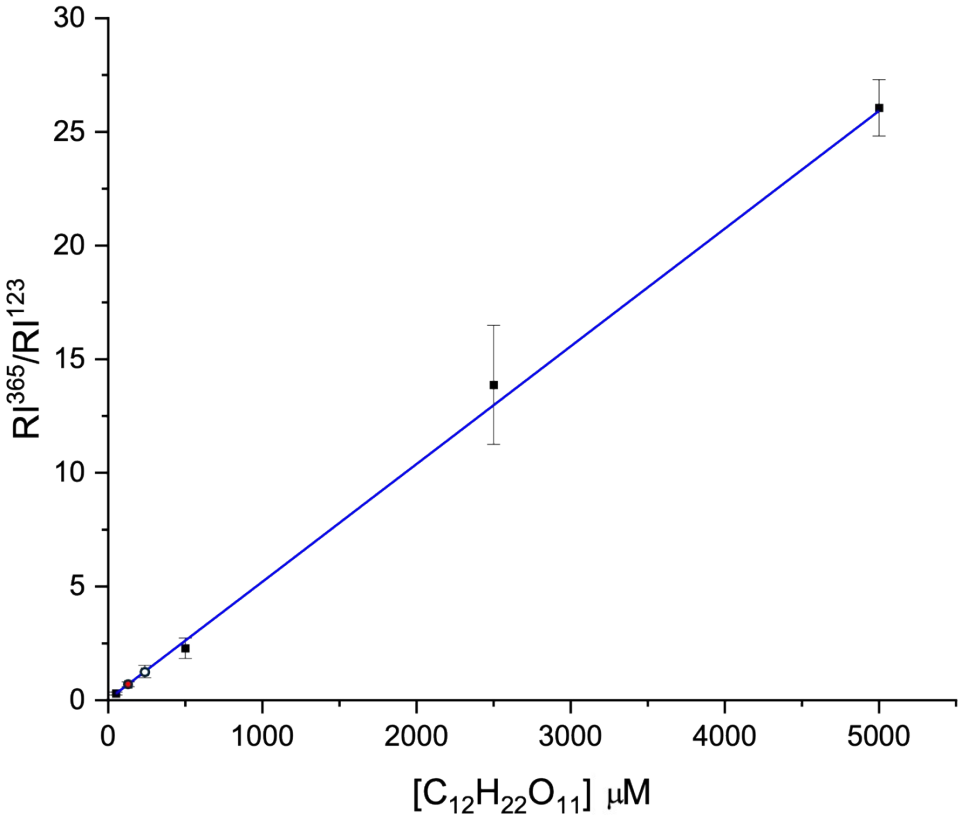

Figure S24: Standard curve for increasing glucose disaccharide concentration where red and white correspond to the 250 I.D. micron capillary and yellow 50 I.D. micron capillary experiments respectively.

References:

1 S. Zapfe and D. Müller, *Rapid Commun. Mass Spectrom*, 1998, **12**, 545–550.
2 R. E. March and C. J. Stadey, *Rapid Commun. Mass Spectrom.*, 2005, **19**, 805–812.
3 J. P. Heindel, R. A. LaCour, and T. Head-Gordon, *Nat. Commun.*, 2024, **15**, 3670.
4 A. Özdemir, J. L. Lin, Y. S. Wang and C. H. Chen, *RSC Adv*, 2014, **4**, 61290–61297.
5 J. T. Maze, T. C. Jones, and M. F. Jarrold, *J. Phys. Chem. A*, 2006, **110**, 12607–12612.
6 M. de la Puente and D. Laage, *J Am Chem Soc*, 2023, **145**, 25186–25194.
7 H. Wei, E. P. Vejerano, W. Leng, Q. Huang, M. R. Willner, L. C. Marr and P. J. Vikesland, *Proc Natl Acad Sci U S A*, 2018, **115**, 7272–7277.
8 E. V. da Costa, A. S. P. Moreira, F. M. Nunes, M. A. Coimbra, D. V. Evtuguin, and M. R. M. Domingues, *Rapid Commun. Mass Spectrom.*, 2012, **26**, 2897–2904.
9 H. T. Huynh, H. T. Phan, P. J. Hsu, J. L. Chen, H. S. Nguan, S. T. Tsai, T. Roongcharoen, C. Y. Liew, C. K. Ni, and J. L. Kuo, *Phys. Chem. Chem. Phys.*, 2018, **20**, 19614–19624.
10 B. J. Bythell, M. T. Abutokaikah, A. R. Wagoner, S. Guan and J. M. Rabus, *J Am Soc Mass Spectrom*, 2017, **28**, 688–703.
11 H.-S. Nguan and C.-K. Ni, *J. Phys. Chem. A*, 2022, **126**, 8799–8808.